PCCP

Cite this: *Phys. Chem. Chem. Phys.*, 2011, **13**, 12249–12253

www.rsc.org/pccp

PAPER

A combined experimental inelastic neutron scattering, Raman and *ab initio* lattice dynamics study of α-lithium amidoborane†

Kate R. Ryan,[ab] A. J. Ramirez-Cuesta,[a] Keith Refson,[a] Martin O. Jones,[ab] Peter P. Edwards[b] and William I. F. David*[a]

Received 2nd March 2011, Accepted 4th May 2011
DOI: 10.1039/c1cp20587k

A combination of inelastic neutron scattering (INS) spectroscopy and Raman spectroscopy with periodic density functional theory calculations is used to provide a complete assignment of the vibrational spectra of α-lithium amidoborane (α-$LiNH_2BH_3$). The Born charge density and the atomic motion up to the decomposition temperature have been modelled. These models not only explain the nature of bonding in α-$LiNH_2BH_3$ but also provide an insight into the atomic mechanisms of its decomposition. The (INS) measurements were performed in the range of 0–4000 cm^{-1} on the high-resolution time-of-flight TOSCA INS spectrometer at the ISIS Spallation Neutron Source at the Rutherford Appleton Laboratory.

Introduction

Lithium amidoborane ($LiNH_2BH_3$), is a promising candidate as a solid state hydrogen store and has been the focus of considerable worldwide research.[1,2] It is a crystalline molecular solid with two known polymorphs[3] containing 13.7 wt% hydrogen and is stable under an inert atmosphere at atmospheric conditions. Lithium amidoborane offers a number of significant advantages over its extensively studied parent compound, NH_3BH_3, that include suppressed borazine release and a lower dehydrogenation temperature of 90 °C.[1]

Developing an atomistic explanation of decomposition mechanisms is key to a full understanding of the performance of hydrogen storage materials and this is not yet fully understood for $LiNH_2BH_3$.[1,2,4,5] In this paper, we present vibrational spectra of α-$LiNH_2BH_3$ obtained from a combination of Raman and inelastic neutron scattering (INS) spectroscopies and provide a complete assignment of the spectra based on periodic density functional theory (periodic-DFT). These studies give a complete description of the atomic vibrations of α-$LiNH_2BH_3$ and highlight the principal atomic motions that occur immediately below the decomposition temperature. This, in turn, provides an insight into the mechanism of decomposition.

Experimental

Schlenk line methods were used for the solution-based preparation. Lithium amidoborane was synthesised *via* the direct reaction of the solid powders of lithium hydride (LiH 95%) and ammonia borane (NH_3BH_3 97%) in a 1 : 1 molar ratio. Dry diethyl ether (Et_2O) was added with rigorous stirring and the mixture left to stir at room temperature for two days. The mixture was then filtered and pumped dry to remove the Et_2O for 5 h on a high vacuum line whilst warming in an oil bath to 50 °C. Diethyl ether was dried by standard methods and distilled before use. All chemicals were purchased from Sigma Aldrich and used without further purification. All handling of materials was performed in an argon atmosphere glove-box (O_2 content <0.1 ppm)

The Raman spectra were recorded on a Jobin Yvon spectrometer (Labram 1B) equipped with a microscope, through a 50-fold magnification objective (Olympus Co.). A 20 mW He–Ne laser (632 nm) was used. The 1800 L mm^{-1} grating provides a resolution that ranges from 1.0 cm^{-1} at 200 cm^{-1} to 0.5 cm^{-1} at 3600 cm^{-1}. The abscissa was calibrated with a silicon standard and the sharp Raman shifts are accurate to ± 2 cm^{-1}. 100 mg of polycrystalline powder was loaded into a glass melting point tube which was flame sealed. The microscope was then focused on the surface of the capillary and spectra were collected over a period of 4 h at 25 °C.

The inelastic neutron scattering (INS) experiments were performed using the high resolution broadband spectrometer TOSCA at the ISIS Spallation Neutron Source at the Rutherford Appleton Laboratory, UK. Full details of the spectrometer have been described elsewhere.[6,7] TOSCA is an inverted geometry time-of-flight spectrometer where a pulsed,

[a] *Rutherford Appleton Laboratory, Harwell Science and Innovation Campus, Didcot, OX11 0QX, UK. E-mail: bill.david@stfc.ac.uk; Fax: +44 (0) 1235 445383*
[b] *Inorganic Chemistry Laboratory, University of Oxford, South Parks Road, Oxford, OX1 0ER, UK*
† Electronic supplementary information (ESI) available. See DOI: 10.1039/c1cp20587k

white beam of neutrons illuminates the sample at 17 m from the source. The backscattered neutrons are Bragg reflected by a pyrolytic graphite analyser and those with a final energy of $\sim$32 cm^{-1} pass through to the ^{3}He detector bank. The INS spectra of the empty aluminium sample holder and a flat background have been subtracted and the raw data were corrected to obtain $S(Q;\omega)$ using standard routines available at ISIS.

Measurements were performed in neutron energy loss mode. Ideally, a ^{11}B enriched sample should be used to eliminate the high neutron absorption of natural boron. However, TOSCA covers an extended energy transfer, E, range: 3 meV $< E <$ 500 meV, providing an excellent energy resolution, ΔE, ($\Delta E/E\sim$ = 1.5%) and allows good quality data to be collected despite the natural boron content. One gram of polycrystalline powder was loaded into an aluminium sachet which was sealed in an aluminium can with indium wire and then cooled to $\sim$20 K. The spectrum was recorded for 12h. The INS spectrum is available from the INS database at www.isis.rl.ac.uk/insdatabase.

Periodic density functional theory calculations were carried out using a plane wave basis-set and pseudopotentials as implemented in the CASTEP code.[8–10] The PBE[11] version of the localised density approximation within DFT was used in conjunction with optimised norm conserving Opium pseudopotentials[12] generated using the Qc-tuning method.[13] The Brillouin zone sampling used a 5 × 5 × 4 grid of k-points generated using the Monkhorst–Pack method. Using the experimentally determined crystal structure as a starting point, a full geometry optimization of the internal atomic co-ordinates was performed, with a plane-wave cut-off energy of 850 eV, to reduce the residual atomic forces to less than 1.5 meV Å^{-1}. Phonon modes were calculated using density functional perturbation-theory[10,14] to compute the dynamical matrix at the Γ-point. The CASTEP output includes the atomic displacements for each mode. This enables visualisation of the modes and the generatation of the inelastic neutron scattering spectrum using the program ACLIMAX[15] (available from www.isis.rl.ac.uk/molecularspectroscopy).

Results and discussion

At room temperature, α-$LiNH_2BH_3$ crystallises in the orthorhombic space group *Pbca* with eight molecules per unit cell[1] each on a point of general (8*c*) symmetry (Fig. 1). Each fundamental vibration of the isolated molecule gives rise to 8 factor group modes of the crystal.

To assign the spectra, we have performed density functional theory (DFT) calculations on the complete unit cell using CASTEP.[8–10] Comparison of the observed and calculated bond distances for the complete unit cell with the experimental data shows good agreement: bond distances are generally within 0.02 Å or 2%. The largest deviations are for the N–H bond length where the distances are 3.4%–4.2% longer than the experimental values. A histogram of these values and the full data can be found in the ESI.† The *ab initio* bond angles are generally within 3° of the experimental values, the largest deviation is for the H–N–H bond where the calculated angle is 104.7° *versus* 94.3° (experimental). We conclude that the *ab initio* calculations for the complete unit cell have accurately reproduced the experimental structure.

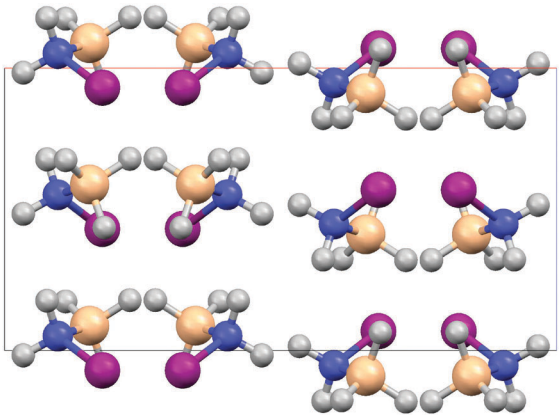

Fig. 1 Structural diagrams of α-$LiNH_2BH_3$ viewing along the *b*-axis Lithium is purple, nitrogen blue, and boron cream.

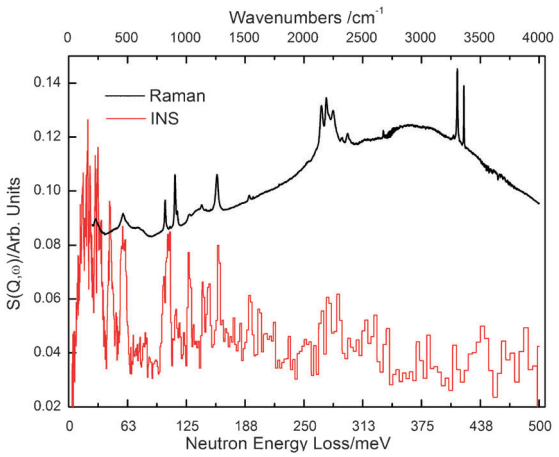

Fig. 2 INS and Raman spectra of polycrystalline α-$LiNH_2BH_3$ in the 0–4000 cm^{-1} region.

Fig. 2 shows the INS and Raman spectra of α-$LiNH_2BH_3$. Similarities and differences are apparent between the two spectra and emphasise the need to have both types of spectra for a complete vibrational analysis. Raman spectroscopy requires a change in polarisability of the molecule and thus is more sensitive to the non-polar motions of the molecule. Moreover, the dynamical information is dominated by heavy atom motions. The INS spectra show all the possible vibrational modes for the structure; in contrast with Raman spectroscopy, there are no selection rules. INS spectra are dominated by the hydrogenic motions, since the intensity of an INS band is proportional to the product of the incoherent scattering cross-section and the amplitude of vibration.[16] As the scattering cross-section for hydrogen is at least 20 times larger than that for all the other atoms present in α-$LiNH_2BH_3$, the INS spectrum emphasises the modes that involve significant hydrogen motion either directly (such as a N–H bend) or where the hydrogen is carried by another atom (*e.g.* torsions).[7] A complete list of all the observed bands and their assignments is provided in the ESI.†

The Raman spectrum as calculated by CASTEP is compared with the experimental spectrum in Fig. 3. It is clear that there is a good agreement between the two, particularly in the

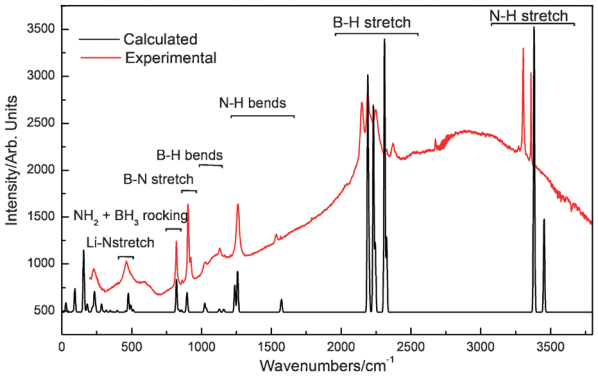

Fig. 3 Comparison of Raman spectra: experimental (red) and calculated by CASTEP for the complete unit cell (black) in the 0–4000 cm^{-1} region.

lower energy region (Li–N stretch experimental and calculated are 231 and 232 cm^{-1} respectively). However in higher energy regions (above 2000 cm^{-1}), the calculation has over estimated the vibrations associated with the B–H and N–H stretching regions, which is a common phenomenon in DFT calculations.

Fig. 4 shows a comparison of the INS spectra calculated from the DFT results and the experimental spectrum. It is clear there is very good agreement between the calculated and observed spectra, although there are some discrepancies with the vibrations involving boron. These are probably due to the presence of ^{10}B in the sample as the DFT calculations are performed using the assumption of ^{11}B. The most notable discrepancy is the lower than predicted intensity for the BH_3 libration band at 362 cm^{-1} and the BH_3 rocking band at 818 cm^{-1}. There is also a shift to higher wavenumbers for the BH_3 wagging modes (1232 cm^{-1} calculated *vs.* 1268 cm^{-1} experimental). This shift to higher wavenumbers most likely arises as a result of the underestimation of the electrostatic forces between the Li^+ and the BH_3 units in the calculation. In the crystal structure, each Li^+ is tetrahedrally coordinated by one NH_2^- and three BH_3 units.[1] These interactions replace the dihydrogen bonding observed in NH_3BH_3[17] as the stabilising factor of the extended structure. Stronger than calculated electrostatic forces further emphasise their importance as the stabilisers of the structure.

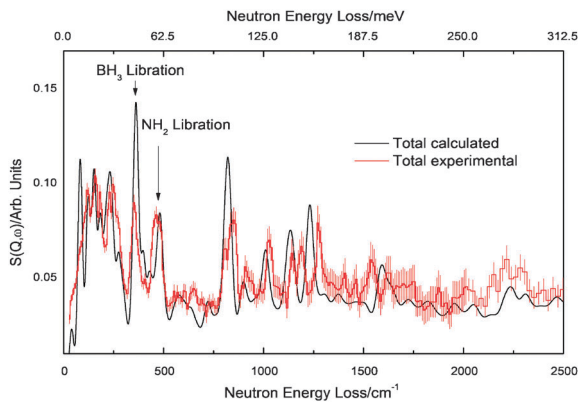

Fig. 4 Comparison of INS spectra: experimental (red) and calculated by CASTEP for the complete unit cell (black) in the 0–2500 cm^{-1} region.

The BH_3 librations occur at lower energies (340–398 cm^{-1}) than the NH_2 librations (416–529 cm^{-1}). This is opposite to those observed for ammonia borane where the onset of NH_3 libration has been shown by NMR and quasielastic neutron scattering (QENS)[18] to have a lower activation energy than for BH_3. This change in behaviour arises due to the close association of the Li^+ and NH_2 in α-$LiNH_2BH_3$. The Li^+ acts as an anchor for its end of the molecule and thus it requires more energy to overcome the electrostatic interactions between the Li^+ and NH_2 and displace the NH_2 unit.

The anharmonicity of certain modes can be explored with a finite displacement calculation. The calculation proceeds by shifting each atom by a small amount, then performing a Self Consistent Field (SCF) calculation to evaluate the forces on the perturbed configuration. Both positive and negative displacements are performed in each direction so that the corresponding force constants can be evaluated using the accurate "central difference" method of numerical differentiation.

Fig. 5 shows the INS spectra generated from the finite displacement calculation on α-$LiNH_2BH_3$ and it is clear that the very low energy modes below 100 cm^{-1} move significantly as the displacement increases. These modes correspond to shearing motions with one half of the unit cell moving rigidly with respect to the other. Indicative of incipient soft modes these modes suggest the possibility of a structural phase transition associated with a lowering of crystal symmetry. No lower symmetry has been observed in α-$LiNH_2BH_3$ down to 10 K. However, the presence of these 'soft' low frequency modes could, indicate a potential structural phase transition at elevated pressures.[19]

Born charges and charge density

Fig. 6 is a schematic drawing displaying the atomic charge ellipsoids for α-$LiNH_2BH_3$. The colours of the atoms correspond to their calculated Born charges depicted by a RWB gradient: tints of blue for high electron density, tints of red for low electron density, white for neutral. The range of values for partial charge was adjusted to the minimum and maximum values present in the calculation. A complete list of all the values is provided in the ESI.†

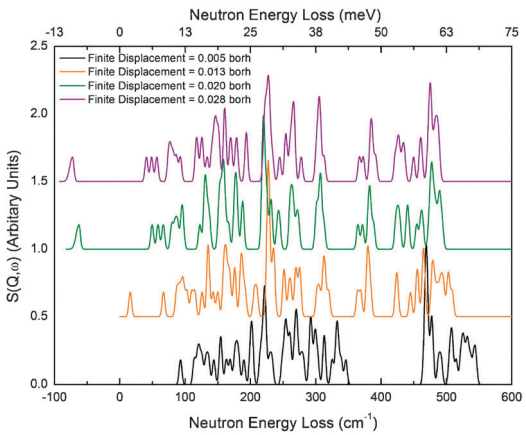

Fig. 5 Graph showing the INS spectra generated from the finite displacement calculation on α-$LiNH_2BH_3$ in the −100–600 cm^{-1} region.

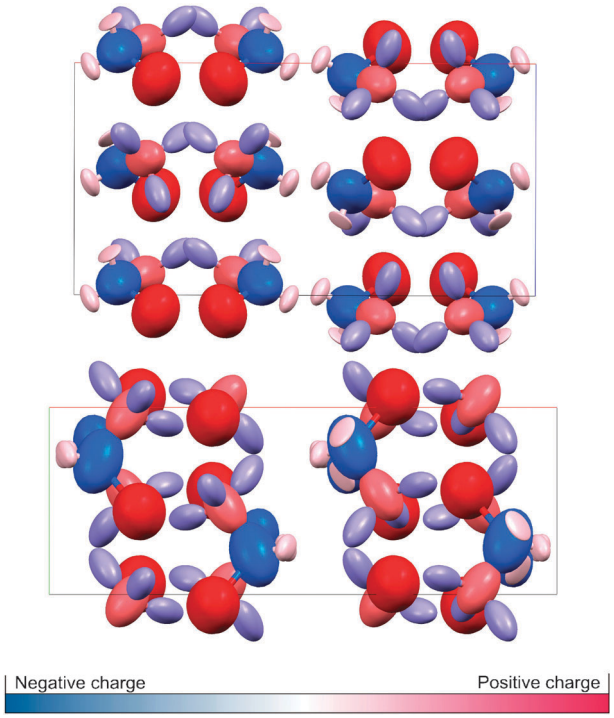

Fig. 6 Structural diagram of α-$LiNH_2BH_3$ viewing along the *b*-axis (top) and the *c*-axis (bottom) showing atomic charge ellipsoids. The colours of the atoms correspond to their calculated Born charges depicted by a RWB gradient: tints of blue for high electron density, tints of red for low electron density, white for neutral.

The partial charge colouring clearly shows the ionic nature of α-$LiNH_2BH_3$ (Fig. 6). The largest charges are located on the Li and N atoms which have charges of +1.02 and −0.97 respectively. The B atom has a partial charge of 0.67 and the hydrogen atoms also have a significant amount of charge. The $H^{\delta+}$ ions (bonded to nitrogen) range between 0.21 and 0.23 and $H^{\delta-}$ (bonded to boron) are between 0.35 and 0.42.

The charge ellipsoids give clear information about the directionality of the *inter* and *intra* molecular bonds. Charge density, in general, is expected to be located along bonds and this is certainly the case with the N, B and $H^{\delta-}$ charge ellipsoids. The majority of the N and B charge density is located along the U_{22} direction of their ellipsoids (associated with the *b*-axis of the unit cell), illustrating the strong dative bond from the lone pair of the N atom to the electron deficient B. The $H^{\delta-}$ charge density is mainly located along the B–H bonds which point towards the Li. The Li^+ charge density, however, is not strongly polarised toward the N atom; this is presumably because the majority of the charge on the N atom is localised in the dative bond. Instead the Li charge density is orientated orthogonally to the N atom and extends between its three nearest BH_3 units. The preference of the Li for bonding towards the BH_3 units rather than the nitrogen atom again emphasises the importance of the Li^+–$H^{\delta-}$ interactions in stabilising the structure of α-$LiNH_2BH_3$.

The $H^{\delta+}$ charge ellipsoids are also orthogonal to the N–$H^{\delta+}$ bond. This unusual orientation is especially obvious when looking at the plane down the centre of the unit cell. The $H^{\delta+}$ form a wall of positive charge between the layers; the charge ellipsoids adopt an orthogonal orientation to maximise the layer–layer separation and minimise repulsion between the layers.

Atomic motion prior to decomposition

In the harmonic approximation, the displacement tensors ${}^{\nu}\boldsymbol{B}_l$ of an atom *l* vibrating in mode ν at temperature *T*/K may be evaluated using the following equation:

$$ {}^{\nu}\boldsymbol{B}_l(T) = {}^{\nu}u_l^2(T) = \frac{16.9}{{}^{\nu}\mu_l\omega_\nu}\coth\left(\frac{1.47\omega_\nu}{T}\right) $$

where the mode frequency, ω, is measured in cm^{-1}, the reduced mass, μ, in atomic mass units and the mean square atomic displacements are in $Å^2$. The individual modes are orthogonal to one another and, in the harmonic approximation, their displacements follow a Gaussian probability distribution. Given the quadrature convolution properties of a Gaussian distribution, the total mean square displacement of an atom at a given temperature may be calculated by summing the contributions of all the individual modes,

$$ B_l(T) = \sum_{\nu} {}^{\nu}B_l(T) $$

Fig. 7 shows how the atomic motions of α-$LiNH_2BH_3$ change with increasing temperature between 100 K and its decomposition at 370 K. No structural phase transitions are observed within this temperature range and the compound decomposes directly to an amorphous state without melting.[20] Fig. 8 gives a quantitative representation of these changes between 100 K and 370 K.

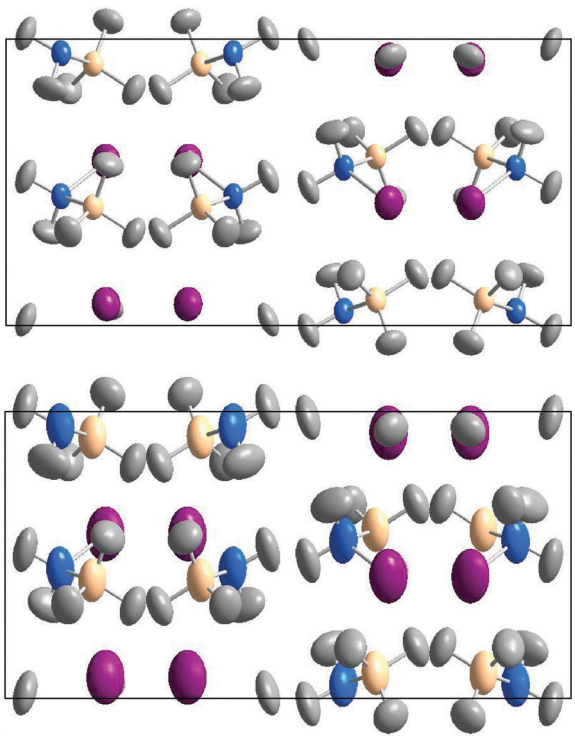

Fig. 7 Structural diagrams of α-$LiNH_2BH_3$ viewing along the *b*-axis showing the total mean square displacement of the atoms at 100 K (top)and 370 K (bottom).

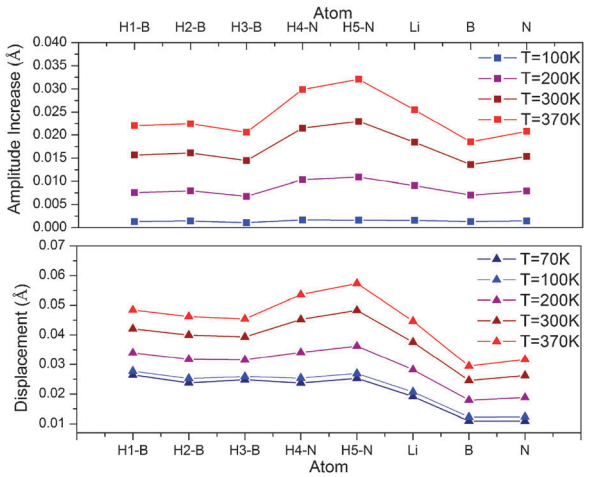

Fig. 8 Graph showing how the atomic displacements of α-$LiNH_2BH_3$ change with temperature between 70–370 K (data given in the ESI†).

From Fig. 7 and 8 it is clear that, of the non-hydrogen atoms, the Li atomic motion changes the most. The motion is essentially spherical at 100 K and changes to a pronounced anisotropic ellipsoidal motion directed predominantly along the *c*-axis at 370 K. The boron vibrations also become more ellipsoidal but along the *a*-axis, orthogonal to the Li motion.

Surprisingly the shape of the hydrogen motion is calculated to change relatively little between 100 K and 370 K (Fig. 7). On first consideration, it might be expected that the hydrogen motion at the decomposition temperature must become considerably anisotropic if the compound is about to decompose and release hydrogen. However, because the decomposition temperature is relatively low (370 K), there is not enough energy to thermally populate the higher energy modes and only the lower energy lattice modes $\leq$ 250 cm^{-1} contribute significantly to the atomic motions. The H atoms bonded to the N (H4 and H5) move a little more than those bonded to the B atom (H1, H2 and H3), possible due to a cooperative motion with the nearby Li atom.

The orthogonal motion of the Li and B atoms is thought to be one of the key factors promoting the low decomposition temperature, causing the crystal to be simultaneously stressed along the *a* and *c*-axes, generating a large amount of strain within the lattice. Thus it seems that by 370 K the amplitudes of these vibrations are sufficiently destabilising to cause the crystal structure of α-$LiNH_2BH_3$ to break down.

Conclusions

The present work provides a complete assignment of the inelastic neutron scattering and Raman vibrational spectra of α-$LiNH_2BH_3$. The TOSCA spectrometer at ISIS is powerful enough to give good intensities and resolution even with samples that contain natural boron. The combination of INS and Raman with DFT calculations together are a potent tool that have been used to provide unambiguous assignments for molecules with complex hydrogenic motion. The DFT calculations result in negative phonon modes which indicate an unstable shearing plane through the centre of the unit cell perpendicular to the *a*-axis. Charge ellipsoids have been modelled to demonstrate the directionality of the *inter* and *intra* molecular bonds. Atomic displacement parameters have been computed up to the decomposition temperature and used to provide insight into the decomposition mechanism which is thought to be initiated by large orthogonal vibrations of the Li and B atoms.

Acknowledgements

The authors would like to thank Tom Autrey, Shawn Kathmann and Greg Schenter of Pacific Northwest National Laboratory, Richland, US for valuble discussions, and the STFC for neutron beam time and access to the super computer SCARF.

Notes and references

1 Z. T. Xiong, C. K. Yong, G. T. Wu, P. Chen, W. Shaw, A. Karkamkar, T. Autrey, M. O. Jones, S. R. Johnson, P. P. Edwards and W. I. F. David, *Nat. Mater.*, 2008, **7**, 138–141.
2 H. Wu, W. Zhou and T. Yildirim, *J. Am. Chem. Soc.*, 2008, **130**, 14834–14839.
3 C. Wu, G. Wu, Z. Xiong, W. I. F. David, K. R. Ryan, M. O. Jones, P. P. Edwards, H. Chu and P. Chen, *Inorg. Chem.*, 2010, **49**, 4319–4323.
4 D. Y. Kim, N. J. Singh, H. M. Lee and K. S. Kim, *Chem.–Eur. J.*, 2009, **15**, 5598–5604.
5 S. Swinnen, V.-S. Nguyen and M.-T. Nguyen, *Chem. Phys. Lett.*, 2010, **489**, 148–153; A. J. Ramirez-Cuesta, M. O. Jones and W. I. F. David, *Mater. Today*, 2009, **12**, 54–61.
6 D. Colognesi, M. Celli, F. Cilloco, R. J. Newport, S. F. Parker, V. Rossi-Albertini, F. Sacchetti, J. Tomkinson and M. Zoppi, *Appl. Phys. A: Mater. Sci. Process.*, 2002, **74**, s64–s66.
7 P. C. H. Mitchell, S. F. Parker, A. J. Ramirez-Cuesta and J. Tomkinson, *Vibrational Spectroscopy with Neutrons With Applications in Chemistry, Biology, Materials Science and Catalysis*, World Scientific, Singapore, 2005.
8 M. D. Segall, P. J. D. Lindan, M. J. Probert, C. J. Pickard, P. J. Hasnip, S. J. Clark and M. C. Payne, *J. Phys.: Condens. Matter*, 2002, **14**, 2717–2744.
9 S. J. Clark, M. D. Segall, C. J. Pickard, P. J. Hasnip, M. J. Probert, K. Refson and M. C. Payne, *Z. Kristallogr.*, 2005, **220**, 567–570.
10 K. Refson, P. R. Tulip and S. J. Clark, *Phys. Rev. B: Condens. Matter Mater. Phys.*, 2006, **73**, 155114–155112.
11 J. P. Perdew, K. Burke and M. Ernzerhof, *Phys. Rev. Lett.*, 1996, **77**, 3865.
12 http://opium.sourceforge.net/sci.html.
13 J. S. Lin, A. Qteish, M. C. Payne and V. Heine, *Phys. Rev. B: Condens. Matter*, 1993, **47**, 4174.
14 X. Gonze, *Phys. Rev. B: Condens. Matter*, 1997, **55**, 10337.
15 A. J. Ramirez-Cuesta, *Comput. Phys. Commun.*, 2004, **157**, 226–238.
16 *TOSCA home page*, http://www.isis.stfc.ac.uk/instruments/tosca/tosca4715.html.
17 N. J. Hess, M. E. Bowden, V. M. Parvanov, C. Mundy, S. M. Kathmann, G. K. Schenter and T. Autrey, *J. Chem. Phys.*, 2008, **128**.
18 N. J. Hess, M. R. Hartman, C. M. Brown, E. Mamontov, A. Karkamkar, D. J. Heldebrant, L. L. Daemen and T. Autrey, *Chem. Phys. Lett.*, 2008, **459**, 85–88.
19 W. Luo, R. Ahuja, Y. Ding and H. K. Mao, *Proc. Natl. Acad. Sci. U. S. A.*, 2007, **104**, 16428–16431.
20 K. R. Ryan, *A study of ammonia borane and its derivatives, (Doctoral thesis)*, 2011.